Available online at www.sciencedirect.com
SCIENCE DIRECT
ELSEVIER
Icarus 180 (2006) 393–402
ICARUS
www.elsevier.com/locate/icarus

Production, ionization and redistribution of O_2 in Saturn's ring atmosphere

R.E. Johnson [a,b,*], J.G. Luhmann [c], R.L. Tokar [d], M. Bouhram [e], J.J. Berthelier [f], E.C. Sittler [f], J.F. Cooper [f], T.W. Hill [g], H.T. Smith [a], M. Michael [a,e], M. Liu [a], F.J. Crary [h], D.T. Young [h]

[a] *Engineering Physics, University of Virginia, Charlottesville, VA 22904, USA*
[b] *Physics Department, New York University, NY 10003, USA*
[c] *Space Sciences Laboratory, University of California Berkeley, CA 94720, USA*
[d] *Space and Atmospheric Science Group, Los Alamos National Laboratory, Los Alamos, NM 87545, USA*
[e] *Centre d'é tude des Environnements Terrestre et Planetaires, Observatoire de St. Maur, 94107 St. Maur, France*
[f] *Goddard Space Flight Center, Greenbelt, MD 20771, USA*
[g] *Department of Physics and Astronomy, Rice University, Houston, TX 77251, USA*
[h] *Southwest Research Institute, 9VTT Information Technology, 02044, San Antonio, TX 78238, USA*

Received 30 April 2005; revised 9 August 2005

Available online 16 November 2005

Abstract

Molecular oxygen produced by the decomposition of icy surfaces is ubiquitous in Saturn's magnetosphere. A model is described for the toroidal O_2 atmosphere indicated by the detection of O_2^+ and O^+ over the main rings. The O_2 ring atmosphere is produced primarily by UV photon-induced decomposition of ice on the sunlit side of the ring. Because O_2 has a long lifetime and interacts frequently with the ring particles, equivalent columns of O_2 exist above and below the ring plane with the scale height determined by the local ring temperature. Energetic particles also decompose ice, but estimates of their contribution over the main rings appear to be very low. In steady state, the O_2 column density over the rings also depends on the relative efficiency of hydrogen to oxygen loss from the ring/atmosphere system with oxygen being recycled on the grain surfaces. Unlike the neutral density, the ion densities can differ on the sunlit and shaded sides due to differences in the ionization rate, the quenching of ions by the interaction with the ring particles, and the northward shift of the magnetic equator relative to the ring plane. Although O^+ is produced with a significant excess energy, O_2^+ is not. Therefore, O_2^+ should mirror well below those altitudes at which ions were detected. However, scattering by ion–molecule collisions results in much larger mirror altitudes, in ion temperatures that go through a minimum over the B-ring, and in the redistribution of both molecular hydrogen and oxygen throughout the magnetosphere. The proposed model is used to describe the measured oxygen ion densities in Saturn's toroidal ring atmosphere and its hydrogen content. The oxygen ion densities over the B-ring appear to require either significant levels of UV light scattering or ion transmission through the ring plane.

Keywords: Saturn; Magnetosphere; Atmosphere; Rings

1. Introduction

The Cassini Plasma Spectrometer (CAPS) (Young et al., 2005) and the Ion Neutral Mass Spectrometer (INMS) (Waite et al., 2005) detected thermal O^+ and O_2^+ over Saturn's main ring shortly after Cassini's orbit insertion. CAPS detected the O^+ and O_2^+ on July 1, 2004 over a radial distance range of 1.79 to 2.10 R_S (Fig. 1) and INMS detected the O^+ and O_2^+ from ~2.12–2.2 R_S, where R_S (~60,300 km) is a Saturn radius. Both sets of measurements occurred north of the ring plane with the sun 23.6° south of the ring plane. Tokar et al. (2005) showed that O_2^+ extends into the magnetosphere inside the G-ring and energetic O_2^+ was observed throughout the magnetosphere (Krimigis et al., 2005). Based on these measurements, O_2^+ is present in densities greater than expected in all regions of Saturn's magnetosphere. Therefore, in addition to the hydrogen (Shemansky and Hall, 1992), OH (Jurac et al., 2002) and nitrogen toroidal atmospheres (Smith et al., 2004), molecular oxygen torii are important components of Saturn's magnetosphere.

* Corresponding author. Fax: +1 434 924 1353.
E-mail address: rej@virginia.edu (R.E. Johnson).

0019-1035/$ – see front matter
doi:10.1016/j.icarus.2005.08.021

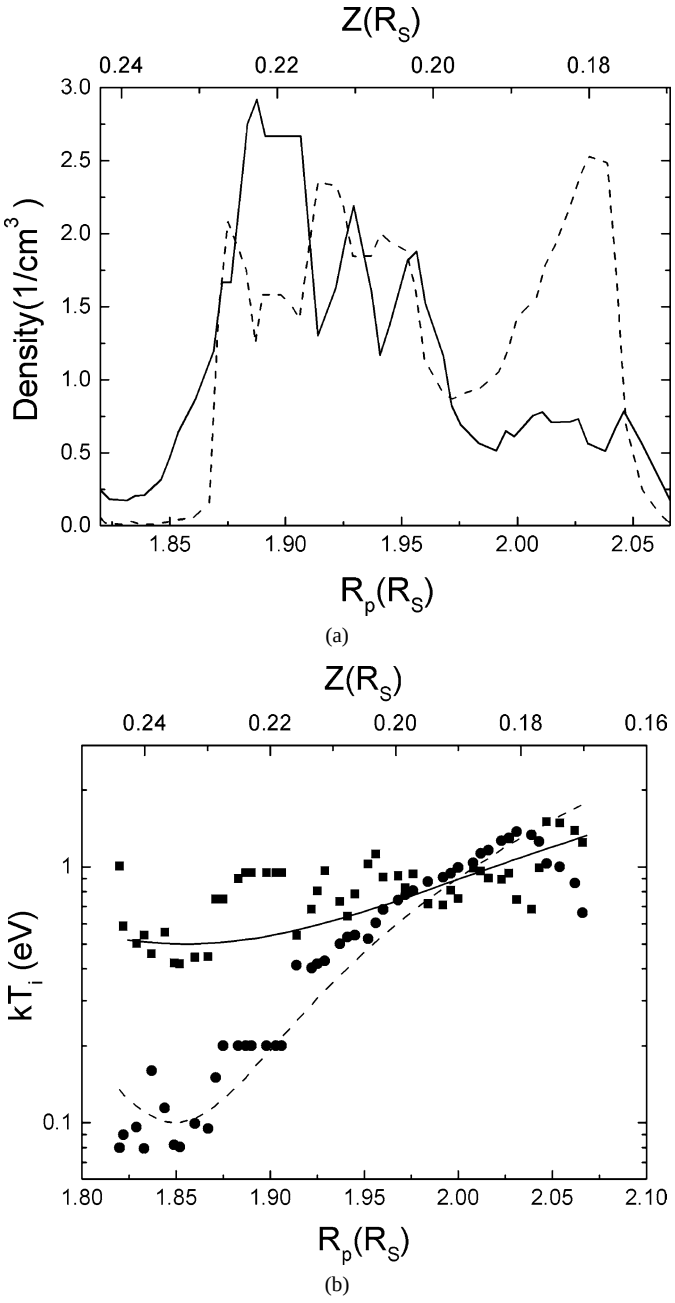

Fig. 1. $O_2{}^+$ and O^+ densities and temperatures vs distance along the equatorial plane R_p in R_S: the O^+ can contain some OH^+ [adapted from Tokar et al. (2005)]. (a) O^+ (solid) and $O_2{}^+$ (dashed) densities at the spacecraft altitude measured by CAPS. Over the B-ring the ion density was less than the electron density as determined by the plasma wave experiments. (b) Measured ion temperatures for O^+ (squares) and $O_2{}^+$ (dots) vs R_p. Lines are the corresponding model temperatures $E_i^* + E_p$.

A toroidal ring atmosphere consisting of water molecules produced by meteoroid impacts (Ip, 1984; Pospieszalska and Johnson, 1991) or photosputtering (Carlson, 1980) had been predicted and the resulting plasma was thought to account for the transient 'spokes' seen over the main rings by Voyager (Grun et al., 1983). Ip (1995) proposed that the gas-phase photo-dissociation of the ejected water molecules produced fragments that resulted in a tenuous O_2 torus ($\sim 10^3$ cm^{-3}) and that $O_2{}^+$ was present in the inner magnetosphere (Ip, 2000, 2005). Whereas water molecules and their fragments stick or react on grains with nearly unit efficiency, any O_2 that is formed does not. Therefore, O_2 can accumulate over the rings, similar to its accumulation over the surfaces of Europa and Ganymede (Shematovich et al., 2005). Although O_2 can be produced from dissociated water fragments by gas-phase (Yung and McElroy, 1977) and surface (Ip, 1995) processes, at Europa and Ganymede O_2 is a signature of the decomposition of ice by incident energetic ions and electrons, a process often called radiolysis (Johnson et al., 2003, 2004). Decomposition refers to the break down of water into O_2 and H_2. Therefore, like the observation of an 'ozone' feature on Dione and Rhea (Noll et al., 1997), the observation of molecular oxygen ions in Saturn's magnetosphere is a marker for radiation-induced decomposition of the ice grains and the icy bodies that orbit within the magnetosphere. Unlike at Europa and Ganymede, the energetic ion and electron flux onto the main rings is small (Simpson et al., 1980; Cooper, 1983; Chenette et al., 1980; Young et al., 2005; Krimigis et al., 2005). Therefore, we propose that UV photons decompose ice by photolysis, producing a toroidal O_2 atmosphere over the rings that is more robust than that predicted.

Because the neutrals in the oxygen torus are confined to a region closer to the ring plane than where CAPS detected ions, in our model we describe the heating of the freshly formed ions by ion-molecule collisions. We also account for the effect of the northward displacement of the magnetic equator. Although the Cassini Orbiter will not fly over the main rings again during its prime mission, it will pass reasonably close ($\sim 2.5 R_S$) to the edge of the main rings. Because the oxygen from the toroidal ring atmosphere can populate this region and more distant regions of the magnetosphere, a good model of this atmosphere will be needed in order to interpret Cassini plasma data.

2. Oxygen atmosphere

Oxygen atmospheres were predicted to be present on the icy satellites of Jupiter produced by the photolysis of water vapor (Yung and McElroy, 1977) and due to the radiolytic decomposition of ice (Johnson et al., 1982; Johnson, 1990). Thin oxygen atmospheres were eventually detected (Hall et al., 1995; McGrath et al., 2004) that were formed, not by photolysis in the gas-phase, but by the radiolytic decomposition of ice by the energetic charged particle flux (Johnson et al., 2004). Although decomposition of ice also produces molecular hydrogen, it readily escapes Europa's gravitational field while molecular oxygen does not. Therefore, Europa creates a significant hydrogen torus in Jupiter's magnetosphere (Shematovich et al., 2005) but not a very robust molecular oxygen torus (Burger and Johnson, 2004; Hansen et al., 2005). Unlike the jovian icy satellites, the icy Saturn satellites and ring particles have relatively small gravitational effects. Therefore, radiation-induced decomposition of these icy bodies *directly* populates Saturn's magnetosphere, forming toroidal oxygen atmospheres in which the molecules co-orbit with these sources (e.g., Ip, 2005). Although O_2 is not the dominant ejecta produced by the incident radiation, it does not condense at the surface temperatures in

Saturn's system and has an ionization potential smaller than the other water products. Therefore, decomposition of ice is the principal source of O_2 in Saturn's magnetosphere and O_2^+ is a relatively stable species throughout the magnetosphere.

That electronic excitations in ice can decompose water molecules has been known for over 50 years (Johnson et al., 2003). Brown et al. (1982) revived interest in this process by measuring the decomposition induced by energetic ions like those in Jupiter's magnetosphere, a process often referred to as radiolysis (Johnson and Quickenden, 1997). Subsequently, it was shown that O_2 is also produced from ice by Lyman-α photons (Westley et al., 1995) and low energy (6–100 eV) electrons (Sieger et al., 1998). In these laboratory experiments, the formation of O_2 follows the prompt loss of hydrogen from ice. Therefore, after a small initial dose, the irradiated layer of the ice becomes slightly oxidizing, which favors the formation of O_2 and oxygen-rich species in the icy surface (Johnson et al., 2003).

Although the fluxes are very low, cosmic ray and energetic particles at MeV to GeV energies are the dominant sources for ionization in the main ring particles. Any O_2 produced in the bulk by penetrating radiation can, in principal, be released by collisions and meteoroid bombardment. However, the energy deposition rate $\sim$0.3 GeV/cm^2/s based on Pioneer 11 data (Cooper et al., 1985) gives an upper limit to the steady state cosmic ray production of O_2 (Cooper et al., 2001; Johnson et al., 2003) that is an order of magnitude smaller than UV-induced decomposition. Energetic magnetospheric particles interact at rapidly declining flux levels with icy bodies at the outer edge of the A ring (Simpson et al., 1980; Eviatar et al., 1983; Paranicas et al., 1997) and with bodies in the F and G rings at higher flux levels (Maurice et al., 2004), partially accounting for O_2^+ observations inside the G ring (Tokar et al., 2005). However, the low plasma temperatures and densities over the main rings suggest that photolysis of ice is the principal source of O_2 gas above the main rings.

The yield for the production of O_2 from ice by Lyman-α photons was measured by Westley et al. (1995) (Table 1). Using the Lyman-α flux at Saturn, the source rate for production of O_2 from ice is: $S_{O_2} \cong 10^6$ O_2/cm^2/s (Johnson et al., 2003). We have assumed that the yield varies nearly inversely on the incident angle (e.g., Johnson et al., 2003) roughly canceling the projection effect on the ring plane. Since photons with lower energies can also produce molecular O_2 from ice ($\sim$6 eV; Orlando and Grieves, 2005; Orlando and Sieger, 2003), this is a *lower limit* to S_{O_2}. Additional measurements are in progress to more carefully examine these issues.

Using available G-values (Johnson et al., 2003; Cooper et al., 2001), the energetic secondary particles produced from the rings by galactic cosmic rays, and observed by Pioneer (Simpson et al., 1980; Maurice et al., 2004), produce more than an order of magnitude less O_2 than does the flux of inner radiation belt ions impacting the edge of the main rings. Water vapor produced by meteoroid impacts or UV desorption, or water coming from regions outside the rings is also photo-dissociated by UV radiation. However, the resulting radicals rapidly stick to the ring particle surfaces. Therefore, any contribution such radicals might make to S_{O_2} would also be by UV photon-induced desorption from the surfaces of the ring particles. Since most of the solar UV is absorbed by the ring particles, and not in an ambient gas, in the following calculations we use the Lyman-α-induced production rate as a *lower limit* to the O_2 source rate.

Table 1
Data for ring atmosphere

Yield (100 K) (Lyman-α)	0.0003O_2/photon
S_{O_2} $\{S_{H_2}/2\}$	$>10^6$ O_2/cm^2/s
v_o	$18.5(1.85R_S/R)^{1/2}$ km/s
τ_b ($\approx \pi R/v_o$)	1.1×10^4 s ($2R_S$)
τ_{co}	3.9×10^4 s
$\langle v_T \rangle = (8kT/\pi m)^{1/2}$	0.26 km/s for $T = 100$ K
H_{O_2} ($\approx R\langle v_T \rangle / v_o$) $\{H_{H_2}/4\}$	1600 km ($2R_S$)
τ_{io} ($O_2 + h\nu \rightarrow O_2^+ + e$)	1.1×10^8 s[a]
τ_{ih} ($H_2 + h\nu \rightarrow H_2^+ + e$)	1.0×10^9 s[a]
τ_{ido} ($O_2 + h\nu \rightarrow O + O^+ + e$)	4.0×10^8 s[a] [$\sim$0.5 eV][b]
τ_{idh} ($H_2 + h\nu \rightarrow H + H^+ + e$)	6.2×10^9 s[a]
τ_{do} ($O_2 + h\nu \rightarrow O + O$)	1.7×10^7 s [0.8 eV][a]
τ_{dh} ($H_2 + h\nu \rightarrow H + H$)	6.7×10^7 s [2.5 eV][a]
$\tau'_{O_2} = [\tau_{do}^{-1} + \tau_{ido}^{-1} + \tau_{io}^{-1}]^{-1}$	1.4×10^7 s[a]
$\tau'_{H_2} = [\tau_{dh}^{-1} + \tau_{idh}^{-1} + \tau_{ih}^{-1}]^{-1}$	3.8×10^8 s[a]
[c] τ_{bi}	$\sim 2.0 \times 10^4$ s
[d] τ_{ci} $(k_{io} n_o)^{-1}$	$(0.7 \times 10^4/c_e)$ s (outer edge of B-ring)
[e] τ_s	3.8×10^4 s

[a] Photoionization and dissociation [mean excess energy of O or H]: Huebner et al. (1992) average of quiet Sun and active Sun. Primes: upper bounds to lifetimes (e.g., ignore c_e).

[b] Luna et al. (2005) [mean excess energy of O^+].

[c] Average bounce time for O_2^+ produced near ring plane, mirroring and returning (Luhmann et al., 2005).

[d] Time for collision of an O_2^+ ion with an O_2 near the ring plane obtained using lower limit to the O_2 density, n_o, where c_e, is the enhancement factor discussed in text ($\gtrsim$10). The reaction rate is: $k_{io} = \langle \sigma_{io} v \rangle = 2\pi[\alpha(ze)^2/m]^{1/2} = 7.4 \times 10^{-10}$ cm^3/s where σ_{io} is the Langevin cross section and α the polarizability of O_2.

[e] τ_s Saturn rotation period (ion co-rotation time).

Since the ring particles are not pure water ice, we write the net source rate of O_2 from the sunlit side of the icy rings as $[c_{ice}(1-f)S_{O_2}]$. Here f is the fraction of the sunlight transmitted through the rings, $f = \exp(-\xi/\cos\theta)$, where ξ is the optical thickness of the ring, θ is the angle of incidence of solar UV flux to the ring plane, and c_{ice} is the ice fraction in the surface of the attenuating particles. O_2 is ejected with a slightly non-thermal energy distribution [$\sim U/(E+U)^2$ with $U = 0.015$ eV; Johnson, 1990]. However, over the A- and B-rings the ejected O_2 has a high probability of adsorbing onto and desorbing from a ring particle in one bounce period, τ_b, ($\sim 10^4$ s), which is about half the orbital period for a neutral (Table 1). Since the photo-dissociation lifetime, τ_{do} ($\sim 2 \times 10^7$ s), is three orders of magnitude larger than τ_b and the residence time (<seconds) of an O_2 molecule on a grain is much shorter than τ_b, the O_2 atmosphere is thermally accommodated to ring particles. Therefore, the gas-phase O_2 will not be hot as assumed by (Ip, 1995) but will have a mean energy $\sim 2\,kT$, where T is average surface temperature of ring particles ($\sim$80–100 K).

Since an O_2 molecule is, on the average, absorbed by the ring particles and re-emitted randomly $\sim 10^3$ times during its

lifetime, the O_2 atmosphere populates *both the shadowed and sunlit* sides of the rings. Using the source rate for the sunlit side $[c_{\rm ice}S_{O_2}(1-f)]$ and an O_2 lifetime, τ_{O_2}, then the average neutral column densities on either side of the rings is

$$N_{O_2}(R) \approx c_{\rm ice}S_{O_2}\tau_{O_2}\big[(1-f)/(1+f)\big]. \quad (1)$$

The quantity $[(1+f)/\tau_{O_2}]$ in Eq. (1) is the average photo-destruction rate of O_2 for the sunlit and shaded sides of the ring plane. Because O from photo-dissociation of O_2 rapidly adsorb onto ring particle surfaces, the ring-atmosphere is primarily molecular. Based on the values of f in Table 1, and ignoring differences in $c_{\rm ice}$, this atmosphere is most dense over the B-ring and least dense over the Cassini gap and C-ring. These densities are somewhat insensitive to the solar conditions because both the source and loss processes depend on the UV flux.

The escape probability for thermal O_2 from the region of the rings is small so that the vertical distribution can be roughly described by

$$n_{O_2}(z,R) \approx n_o(R)\exp\big[-(z/H_{O_2})^2\big], \quad z \ll R_S, \quad (2)$$

where z is the height above the ring plane and R is the distance from Saturn. The density in the ring plane, n_o, is $\sim[(2/\pi^{1/2})(N_{O_2}/H_{O_2})]$, and the centrifugal scale height for neutrals is $H_{O_2} \approx R\langle v_T\rangle/v_o(R)$, where $\langle v_T\rangle[=(8kT/\pi m)^{1/2}]$ and $v_o(R)$ is the Keplerian orbital speed (Johnson, 1990; Ip, 1995). For an average ring particle surface temperature $\sim$100 K, $\langle v_T\rangle$ is 0.26 km/s for O_2, in which case $H_{O_2} \approx$ 1600 km at $2R_S$ and varies roughly as $R^{-3/2}$. Therefore, in the absence of additional heating processes, the atmosphere lies below the magnetic equator, located $\sim$2500 km north of the ring plane, and well below the spacecraft altitudes at which CAPS detected oxygen ions (0.15–0.25R_S corresponding to $\sim$9000–15,000 km).

Using an O_2 lifetime determined by ionization and dissociation [$\tau_{O_2} \approx \tau'_{O_2}$: Table 1], lower limits to N_{O_2} can be obtained (Table 2). Such estimates ignore edge effects due to the high inclination of the Sun during Cassini SOI, and radial transport. These would smooth over the variations in the optical thickness and density, particularly at the Cassini gap which is only $\sim$3 scale heights wide. Recycling of O_2^+, O^+ and O on the grain surfaces increases τ_{O_2} as shown below. Since the ring atmosphere was not directly detected, ion production and loss are first described.

3. Ion column densities

Although the O_2 densities are assumed to be similar on the sunlit and shaded sides of the ring plane, the ion densities are not. Photo-ionization of O_2, which produces both O_2^+ and O^+ (Table 1), is reduced on the shaded side by the optical thickness of the rings. Unlike O_2 the ion lifetimes are short due to collisions with ring particles, leading to neutralization or surface reactions. The newly formed ions attempt to move between mirror points that are symmetric with respect to the magnetic equator, which is shifted north of the ring plane, affecting the asymmetry.

The observed ions have small gyro-radii, r_g (<0.1 km for O_2^+) and have a probability, f_i, for surviving passage through the rings. The column densities on the sunlit, N_{si}, and shaded, N_{shi}, sides of the rings can be described by two rate equations:

$$dN_{si}/dt \approx N_{O_2}/\tau_i - N_{si}/\tau_{si} + N_{shi}f_i/\tau_{si}, \quad (3a)$$

$$dN_{shi}/dt \approx N_{O_2}f/\tau_i + N_{si}f_i/\tau_{shi} - N_{shi}/\tau_{shi}. \quad (3b)$$

The first terms describe the ionization of the neutrals where τ_i is the ion formation time, either τ_{io} for O_2^+ production or τ_{id} for O^+ production. Values are given in Table 1. The second and third terms on the right are due to transport across the ring plane, where τ_{si} and τ_{shi} are the times spent on either side before crossing the ring plane. In this model, ion loss is assumed to occur primarily by interaction with the ring particles through $(1-f_i)$. *Ignoring the dipole offset*, then $\tau_{si} \sim \tau_{shi} \sim \tau_{bi}$, where τ_{bi} is the average bounce time, about half the time between mirror points (e.g., Luhmann et al., 2005).

Solving Eqs. (3), the steady state column densities are

$$N_{si} \approx N_{O_2}(\tau_{bi}/\tau_i)(1+ff_i)\big/\big(1-f_i^2\big), \quad (4a)$$

$$N_{shi} \approx N_{O_2}(\tau_{bi}/\tau_i)(f_i+f)\big/\big(1-f_i^2\big), \quad (4b)$$

where, again, f is the fraction of light penetrating the rings. The singular behavior at $f_i = 1$, resulting from our neglect of loss processes other than ring absorption, is not a problem because in practice $f_i < 1$ over the main rings. Inserting N_{O_2} from Eq. (1), the ion column densities above and below the ring plane are proportional to the ratio of the lifetime for O_2 destruction to the ionization lifetime, $[\tau_{O_2}/\tau_i]$, which is, roughly, independent of solar conditions. In addition, if the ion transmission efficiency, f_i, and the ion bounce time, τ_{bi}, are similar for O^+ and O_2^+, then the ratio of the O^+ to O_2^+ column densities on either side of the ring plane is equal to the *branching ratio*

Table 2
Ring atmosphere parameters: solar zenith angle $\sim$66°

Rings (extent)	A (2.27–2.03R_S)	Cassini (2.03–1.95R_S)	B (1.95–1.53R_S)
Area (10^{20} cm^2)	0.55	0.18	0.97
$\xi(f)$[a]	0.6 (0.23)	0.12 (0.74)	1.6 (0.02)
$[1-f]/[1+f](xf)$[b]	0.63 (0.14)	0.15 (0.11)	0.96 (0.019)
N_{O_2} (10^{13} O_2/cm^2)[c]	$>0.4c_ec_{\rm ice}$	$>0.1c_ec_{\rm ice}$	$>0.7c_ec_{\rm ice}$

[a] Rough average optical depth, ξ, and, brackets, transmission factor, f, using 66° zenith angle.
[b] Factor in Eq. (1); brackets: factor in Eq. (4b) for $f_i = 0$.
[c] O_2 column density using Eq. (1) with $\tau_{O_2} = c_e\tau'_{O_2}$ at mean solar activity where c_e is the ratio of the escape efficiency of H relative to O and $c_{\rm ice}$ is the fraction of the ring particle composition that is ice: this is lower for the particles in the Cassini division and the C-ring than either the A- or B-rings.

for ionization, which is ∼0.24–0.30 depending on solar activity (Table 1).

The ratio of the steady state column densities is determined by the optical thickness of the rings to both ions and UV-photons:

$$N_{\rm shi}/N_{\rm si} \approx (f_i + f)/(1 + f f_i). \quad (5)$$

The ability of the ions to wend their way through the rings, f_i, is determined roughly by ξ, the ion's pitch angle and gyroradius, and, possibly, the charging of the ring particles. If all ions are absorbed on crossing the ring plane, then $f_i = 0$ and the column density ratio is $\sim f$, the photon penetration efficiency. Ignoring scattered light, the oblique incidence [$\cos^{-1}(\theta) = 2.5$ at SOI] causes f to be very small over the B-ring so the density ratio, $\sim(f_i + f)$, can be dominated by ion transmission. Note that, if f_i for ion transmission is also small, then the column density over the Cassini gap on the shaded side of ring would be *larger* than that over the B-ring, opposite to the neutral density. Scattered light and oblique incidence through the Cassini gap, allowing illumination of the gas above the A- and B-rings, can smooth over these differences. Since Cassini was also in Saturn's shadow during the CAPS measurement period, simulations will eventually be required.

4. Dipole offset and ion-molecule collisions

The ion energy in the corotating frame is, roughly, $E_i^* + E_p$, where E_i^* is ion energy at formation and E_p is the pick-up gyro-energy, $\sim m_i(v_{\rm co} - v_o)^2/2$. E_i^* is the initial thermal energy, E_i, plus the energy it attains due to formation off the equator. Whereas O^+ is formed 'hot' ($E_i \sim 0.5$ eV at peak), exhibiting a range of pitch angles and mirror altitudes, the newly formed $O_2{}^+$ ($E_i \sim 2$ kT) has pitch angles $\sim\pi/2$. Therefore, accounting for the off-set dipole, $O_2{}^+$ will initially have northern mirror points in the vicinity of $z_m \sim 0.08 R_{\rm S} \sim 5000$ km. This results in a vertical scale much larger than that for neutral O_2, but *well below* the region measured by CAPS (∼9000–15,000 km north). Therefore, the dipole offset alone cannot account for the CAPS measurements. The $O_2{}^+$ ions must have been either scattered, heated or affected by electric fields prior to detection. Here we show that ion-molecule collisions alone can give mirror latitudes sufficiently large to account for the CAPS measurements.

Over the A- and B-rings, where the neutral density is large, the ion-molecule collision time ($\tau_{\rm ci}$), obtained using estimates of c_e below, is short compared to the ion bounce time, $\tau_{\rm bi}$ (Table 1). Therefore, newly formed ions can be scattered by O_2 before they leave the formation region. After mirroring, these ions can again be scattered as they move obliquely through the neutral cloud. At these distances from Saturn, the relative collision speed is low, so that the ion and molecule can orbit each other before separating. The cross section for such a collision is determined by the polarizability of O_2. This results in a collision time, $\tau_{\rm ci}$, that is independent of the relative velocity (Johnson, 1990; Table 1). For $O_2{}^+ + O_2$ collisions, elastic scattering and charge exchange are indistinguishable. Therefore, the scattered

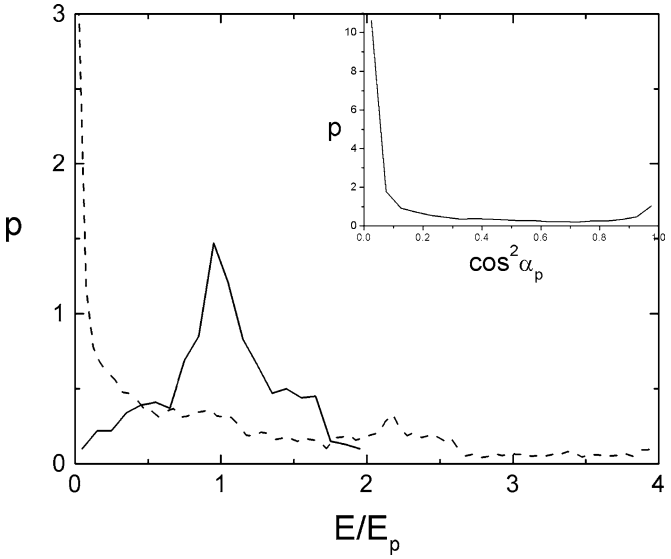

Fig. 2. Distribution function, p, of energies following an $O_2{}^+ + O_2$ collision in which orbiting occurred. Exiting ion energies are given in the rotating frame (solid) and neutral energies in the Kepler orbit frame (dashed line). Both are given as a fraction of the pick-up gyro-energy, E_p. Note: these essentially define an ion/neutral 'temperature' which is of the size of $(v_{\rm co} - v_o)$ hence independent of R. (The insert shows the pitch angle distribution, p, as a function of $\cos^2\alpha_p$: average $\cos^2\alpha_p$ is 0.23; loss cone located at, $\cos^2\alpha_p \sim 0.8$ near the inner edge of the B-ring and ∼0.95 near the outer edge of the A-ring.)

ion attains a new velocity equal to the velocity of the center of mass in the inertial frame plus a velocity in a random direction that is equal to half the relative collision speed. For such collisions, it is seen in Fig. 2 that the scattered ions attain a broad distribution of energies in the rotating system, but with a 'thermal' energy about equal to the initial pick-up energy. Since the neutral O_2 can also attain quite large energies, as indicated in Fig. 2, it can be scattered into regions outside of the main rings (Fig. 3), possibly accounting for the $O_2{}^+$ detection just beyond the main rings by Tokar et al. (2005).

Because $v_{\rm co}$ and v_o are not very different over the ring plane, the average energy of the scattered ions in the rotating frame is comparable to the initial gyro-energy, E_p (Fig. 2). This is remarkably consistent with the measured ion temperatures (Tokar et al., 2005). However, energies larger than the initial pick up energy, E_p, and pitch angles very different from $\pi/2$ occur as seen in Fig. 2. These results are independent of the relative collision speed and, hence, are independent of R. Although the focus above is on $O_2{}^+$, O^+ can also be scattered in ion–molecule collisions. Luhmann et al. (2005) simulated the ion motion in the presence of the dipole field with gravity, and included the scattering of both $O_2{}^+$ and O^+.

Here we note that, ignoring centrifugal confinement, the magnetic latitude of the mirror point, λ_m, for an ion formed at λ with a pitch angle α_p, can be approximated by $\lambda_m^2 \approx \lambda^2 + (2/9)\cos^2\alpha_p$ when λ_m and λ are small. This corresponds to an altitude for the northern mirror point, $z_m \sim [0.04 R_{\rm S} + \lambda_m L R_{\rm S}]$. In regions where the scattering probability is small, α_p is $\sim\pi/2$ and $z_m \sim 0.08 R_{\rm S}$ (∼5000 km) as discussed above. On the other hand, for scattered $O_2{}^+$, the average value of $\cos^2\alpha_p$ in Fig. 2 is ∼0.23. This corresponds to a mirror latitude $\lambda_m \sim 0.22$ ra-

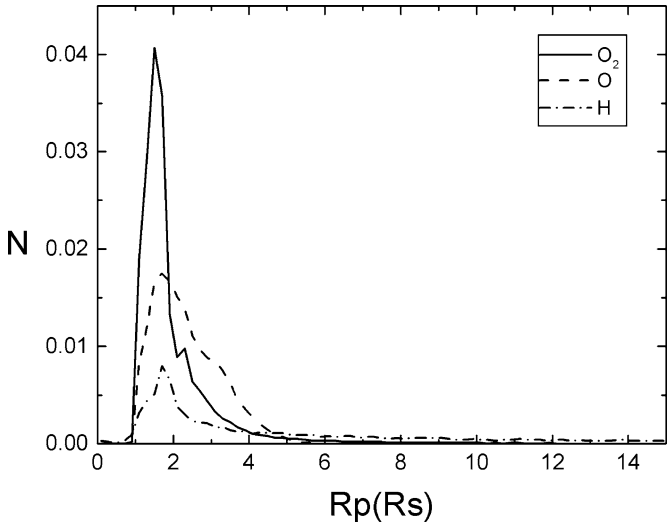

Fig. 3. Snapshot of the distribution of O (solid) and H (dashed) from dissociated O_2 and H_2 respectively and the distribution of O_2 from $O_2^+ + O_2$ collisions. These are formed close to the ring plane and a snap shot of the instantaneous distribution is given as a column density normalized to one vs distance R_p along the equator. The production rate over each region of the ring is proportional to the factor $[(1-f)/(1+f)]$ in Table 2 and $c_{\rm ice}$ is assumed to be the same in each region. The probability of hitting the rings is proportional to $(1-f)$. The fractions of each of the particle populations outside the ring region ($R > 2.27R_S$), including escape, for the H, O, and O_2 distributions are ∼0.9, ∼0.6, and ∼0.4. The ratios are smaller than the simple model ($\Delta E/E_o$) in the paper because the particles are produced close to the ring plane. Simulations are in progress to account for the differences in the vertical distribution for hydrogen and oxygen.

dians so that ions can attain altitudes well above the Cassini trajectory.

The effect of centrifugal confinement can be estimated using the ion scale height. This is written as $H_i \sim [2kT_i/3m_i\Omega^2]^{1/2}$, where T_i and m_i are the ion temperature and mass and Ω is the angular velocity (Hill and Michel, 1976). Even though the velocity distribution of the scattered ions is not fully isotropic, their mean kinetic energy is close to the initial gyro energy (Fig. 2) so that $kT_i \sim E_i^* + E_p$, which roughly fits the measured temperatures in Fig. 1. Therefore, H_i increases as $[\sim(1 - v_o/v_{\rm co})R]$ for R greater than R_x, which is the equatorial radius where the Kepler orbit speed equals the co-rotation speed. To roughly account for the effect of the electrons and other ions via the electric fields Bagenal and Sullivan (1981) write $m_i \to (m_i - m^*)$ where m^* is a function of the electron and ion temperatures and densities. Due to their frequent interaction with the ring particles, the electron temperature is small over the dense regions of the main rings. If the electron temperatures are comparable to or larger than the ion temperatures, then $m^* \neq 0$ and the fields affect the ion motion. Assuming, initially, that $m^* \sim 0$ then the H_i for O_2^+ and O^+ are ∼0.18 and $0.22R_S$ respectively at $R \sim 2.05R_S$, the end of the CAPS data (Fig. 1) and go to a minimum at R_x. Since the scale heights are smaller than the average mirror altitudes estimated above over most of the measurement region, the vertical distribution of ions for $R > R_x$ is primarily determined by centrifugal confinement consistent with simulations (Luhmann et al., 2005; Bouhram et al., 2005).

5. Oxygen recycling and hydrogen atmosphere

Atomic oxygen produced by photo-dissociation has an average energy ∼0.8 eV (Table 1). This is much smaller than the orbital energies near the inner edge of the C-ring and the outer edge of the A-ring [2.6 and 1.4 eV/amu, respectively]. Therefore, most of the O produced from the principal O_2 loss processes returns to the surfaces of the ring particles. In addition, O_2^+ and O^+ can neutralize or react on these surfaces, so that atomic and molecular oxygen ions and the oxygen atoms can, *in principle*, be recycled into O_2 on a ring particle surface. Although the oxygen chemistry at the surface is complex, the rate for adsorbed oxygen to be eventually recycled as O_2 is controlled by the ratio of H to O in surface layers of ring particles. It has been shown, however, that this ratio is only slightly different from 2:1 for ice under irradiation (Rye et al., 1978; Brown et al., 1980). Therefore, *in steady state*, the chemical details can be ignored and the recycling of adsorbed oxygen back to O_2 is determined by the relative efficiencies for the net loss of hydrogen and oxygen *from the ring/atmosphere system*.

In laboratory experiments on fresh ice samples, hydrogen is lost preferentially creating a surface which is very slightly oxygen rich, after which H_2 and O_2 are produced in a ∼2:1 ratio (e.g., Johnson et al., 2003). Since the energy spectrum for the desorbed H_2 is close to thermal, H_2 does not directly escape from the ring atmosphere. Assuming an H_2 source rate twice that for O_2, densities for H_2, H, H_2^+, and H^+ can also be estimated using the model above. That is, H atoms, like O, stick to the grain surfaces, whereas H_2 rapidly desorbs with unit efficiency and accumulates in the atmosphere. Using only the lifetimes in Table 1, the H_2 *column density* would be about an order of magnitude larger than that for O_2 and the H_2^+ *column density* would be comparable to that of O_2^+. However, the H_2 scale height is about four times that for O_2 and the relative loss rates differ. Because of the long lifetimes for O_2 and H_2, these loss rates, although small, are important.

The loss of hydrogen and oxygen to Saturn's atmosphere and to the inner magnetosphere can be roughly estimated from the average excursion distance outside the ring system. This distance is roughly given by $\Delta R \sim [\Delta E/E_o]R$, where ΔE is the energy given to an atom or molecule which had an orbital energy E_o. Hydrogen is more weakly 'bound' in the ring system; that is, its E_o is smaller than that for oxygen at the same orbital radius. In addition, the average energy of H following dissociation of H_2 is three times larger than that for O derived from O_2 (Table 1). Therefore, the average value of $[\Delta E/E_o]$ for hydrogen is more than an order of magnitude larger than that for oxygen at the same orbital radius. Using the mean dissociation energies, the cloud of hot H from dissociation is seen to extend farther into the magnetosphere than the cloud of hot O from dissociation of O_2 (Fig. 3) leading to a higher probability of escape and loss to the outer magnetosphere. Therefore, even though H_2 and O_2 are initially produced stoichiometrically (2:1 ratio), steady state is achieved when the oxygen density in the ring atmosphere builds up until its loss rate becomes about half the hydrogen loss rate.

If c_e is the ratio of the loss rate for two hydrogen to the loss rate for one oxygen, we can roughly account for recycling of oxygen on the ring particle surfaces. That is, the effective lifetime for oxygen in the toroidal ring atmosphere becomes $\tau_{O_2} \sim c_e \tau'_{O_2}$. Based on the loss rate estimates above, $c_e \gtrsim 10$. This indicates that the steady state O_2 and O_2^+ column densities and O_2^+ scattering rates are at least an order of magnitude larger than the lower bounds in Table 1. The ratio of O_2^+ to H_2^+ content of the ring cloud in steady state is, roughly, c_e divided by the ratio of ionization times. Therefore, the O_2^+ number density over the main rings is at least an order of magnitude larger than the H_2^+ number density, consistent with the non-detection of H_2^+ by CAPS (Young et al., 2005; Tokar et al., 2005).

6. Summary and comparison to CAPS data

CAPS and INMS instruments on the Cassini spacecraft measured the ionic component of the ring atmosphere vs distance from Saturn at one altitude. Here we developed a model for the neutral and ion ring atmosphere structure consistent with those measurements. Because the energetic particle flux over the main rings is small, a molecular oxygen ring atmosphere is primarily produced by the solar UV flux. This flux is more efficiently absorbed by the ring particles than by the transient water vapor produced by impacts. Therefore, we propose that the decomposition of ice on the surfaces of the ring particles by the solar UV is primarily responsible for the ring atmosphere. Dissociation of transient water vapor (Ip, 1995) and cosmic ray and energetic magnetospheric particles (Maurice et al., 2004) will be smaller additional sources subject to the same physics and chemistry described here. Therefore, the available data for the photo-production of O_2 from ice was used to describe the production of an oxygen torus over Saturn's main rings with the ring particles surfaces are assumed to have an ice fraction c_{ice}.

Although freshly formed and ejected O_2 has a non-thermal energy distribution, O_2 adsorbs and desorbs from the surfaces of the ring particles many times during its lifetime. Therefore, the atmosphere is *a surface boundary layer atmosphere* (Johnson, 2002) with an average temperature determined primarily by the temperatures of the ring particles. The neutral component of the atmosphere is only weakly dependent on solar conditions and is similar above and below the ring plane with the largest column densities over the B-ring. Ion-molecule collisions and photo-dissociation produce a hot component, as is the case for Europa's O_2 atmosphere (Shematovich et al., 2005). This acts to redistribute oxygen, which smoothes the differences between the regions and populates the inner magnetosphere (e.g., Fig. 3), possibly accounting for the Cassini UV observations of oxygen (Esposito et al., 2005). As discussed, the surfaces of the ring particles, which are slightly oxidizing, can act to recycle the oxygen atoms and ions produced by photo-dissociation and ionization of O_2.

Molecular hydrogen is also produced (Johnson et al., 2003), but with a scale height about a factor of four larger than that of O_2. Although the H_2 lifetime against ionization and dissociation is longer than that for O_2, it is also lost more efficiently. In steady state the molecular oxygen atmosphere builds up until the loss of hydrogen and oxygen are, roughly, stoichiometric (2:1). When that is the case, the size of the escape ratio, c_e, suggests that the H_2^+ column density is at least an order of magnitude smaller than the O_2^+ column density, consistent with the CAPS data.

Since the neutral atmosphere peaks close to the ring plane, newly produced O_2^+ ions would have northern mirror points about twice the altitude of the northern offset of the magnetic equator ($\sim 0.08 R_S$). This is larger than the neutral scale height, but is much smaller than the altitude over the B-ring where CAPS detected ions. We propose here that these ions are scattered by collisions with O_2. Although the temperatures of the scattered ions do not differ significantly from the pick-up temperature (Fig. 2), the ions acquire a component of velocity along the field lines resulting in pitch angles that can differ significantly from $\pi/2$ (see insert in Fig. 2). Therefore, the O_2^+ temperature at the spacecraft altitude is reasonably well described by $\sim(E_i^* + E_p)$ (Fig. 1b; Tokar et al., 2005). E_i^* is $\sim$0.1 eV due to the initial thermal energy ($\sim$0.02 eV) and the energy associated with being formed off the magnetic equator ($\sim$0.08 eV). The observed ion temperature exhibits a minimum near R_x, where the Kepler (v_o) and corotation (v_{co}) speeds are equal, and grows as $\sim m(v_{co} - v_o)^2/2$ for larger and smaller R. The temperature of the O^+ ions is also reasonably well described by ($\sim E_i^* + E_p$) (Fig. 1b; Tokar et al., 2005). Since E_i is $\sim$0.5 eV for O^+, pitch angles different from $\pi/2$ occur at all R. Therefore, in the region around R_x, the measured O^+ density is larger than the O_2^+ density at the spacecraft altitude as seen in Fig. 1a. As R increases and altitude decreases, the measured O^+ to O_2^+ density ratio over the edge of the A-ring (Fig. 1a) approaches the branching ratio for ionization (Table 1), consistent with the INMS data (Waite et al., 2005). We ignore here the 'oscillations' in Fig. 1a, which could be real and, possibly, related to the ring structure.

The O_2^+ density in Fig. 1a is seen to grow rapidly near R_x ($v_o \approx v_{co}$). The peak occurs at an altitude $\sim 0.23 R_S$, requiring mirror latitudes $\lambda_m \gtrsim 0.1$ that can be achieved by ion–molecule scattering. The ion density is seen to decrease in going from the peak density over the B-ring to over the inner edge of the A-ring even though the spacecraft altitude is slowly decreasing. This follows the trend for neutral source rate in our model, but not for the ion densities as discussed below. For $R < R_x$ the densities in Fig. 1a are small. This is due, in part, to the higher spacecraft altitudes, but is also due to the fact the gravitational perturbation causes ions to precipitate with high efficiency into Saturn's atmosphere when $R \gtrsim R_x$ (Luhmann et al., 2005). Below we discuss the region $R > R_x$.

Because the ion densities are only measured at one altitude, assumptions about their distribution with z are needed to compare to the model. Two estimates of the ion scale heights are given in Fig. 4a calculated using the ion temperatures, T_i, in Fig. 1b. Over most of the region these scale heights are smaller than the mean altitudes of the mirror points ($\sim 0.22R$) so that centrifugal confinement primarily determines the vertical distribution of the ions. Therefore, the ion *densities and column densities* at the magnetic equator can be estimated from the data

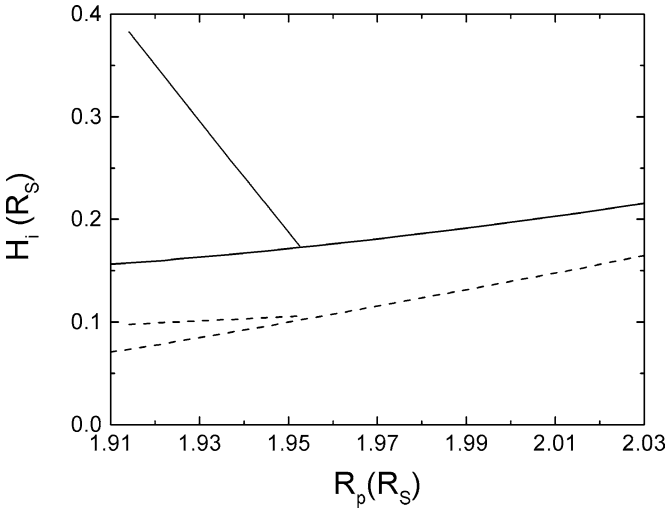

Fig. 4. (a) Estimates of centrifugal scale height, H_i, plotted vs R_p in R_S for ions O^+ (solid) and $O_2{}^+$ (dashed). H_i is calculated using temperatures in Fig. 1b, fit to $kT_i \sim E_i + E_p$ (Tokar et al., 2005) and the expression $H_i \sim [2kT_i/3(m_i - m^*)\Omega^2]^{1/2}$. Lower estimates: assume $m^* = 0$ (i.e., ignore ambipolar fields); upper estimates ($m^* \neq 0$): m^* chosen so that the ratio of $O_2{}^+$ to O^+ column densities is approximately equal to the production ratio (4 to 1); column densities calculated using the measured ion density in Fig. 1a and H_i. (b) Estimates of the column density above the magnetic equator for O^+ (solid) and $O_2{}^+$ (dashed) vs R_p in R_S. Obtained using the scale heights in (a) and the densities in Fig. 1a. Lower curves: ($m^* \neq 0$) and upper curves ($m^* = 0$). Insert: corresponding ion densities at the magnetic equator.

in Fig. 1a using $\exp[-(z/H_i)^2]$ for the variation with altitude. If we first assume that the ions act independently ($m^* \sim 0$ in $H_i \sim [2kT_i/3(m_i - m^*)\Omega^2]^{1/2}$), the lower curves in Fig. 1a are obtained. These values of the scale height determine the upper curves in Fig. 4b. It is seen that the $O_2{}^+$ column density is larger than that for O^+, consistent with the photo-ionization branching ratio. However, the $O_2{}^+$ column density becomes very large with decreasing R over the B-ring due to the very small values of H_i. If the electron temperature is not negligible, then $m^* \neq 0$, modifying the ion altitude profile. To estimate m^*, we constrain the ratio of $O_2{}^+/O^+$ column densities to be about equal to the production ratio from O_2 (∼4; Table 1). This gives an estimate for m^* at each position on the magnetic equator. Using $m^* \neq 0$ results in the larger scale heights in Fig. 4a and smaller densities in Fig. 4b. Therefore, the presence of electric fields (via m^*) has a large affect on our estimate of the $O_2{}^+$ *column density* over the B-ring in Fig. 4b, but a small effect in the Cassini gap and near the inner edge of the A-ring where the spacecraft altitudes are lower and the ion temperatures are larger. Over the region 1.91 to $1.95R_S$, the estimated m^* varies from ∼0.4 to ∼0.1 times the mass of an O_2 molecule, considerably reducing our estimate of the $O_2{}^+$ column density over the B-ring.

The ion column density on the shaded side of the ring plane, N_{shi} in Eq. (4b), is determined by the ring composition, c_{ice}, the enhancement factor for escape of hydrogen relative to oxygen, c_e, and the transmission through the rings for both ions, f_i, and UV photons, f. Comparing the column densities in Fig. 4b to the expression for N_{shi} in Eq. (4b), the ratio of the escape efficiency of hydrogen to oxygen, c_e, is greater than unity at all positions along the magnetic equator. This is consistent with our earlier discussion. Although the ion density at the magnetic equator is very sensitive to the extrapolation in the vicinity of the Cassini gap, the column density is much less sensitive. Using the rough average ion bounce time in Table 1 and assuming f_i is small, the column density extrapolated in the center of the Cassini gap in Fig. 4b implies that $c_e c_{ice}$ in our model is ∼10. If $f_i \sim f$, then $c_e c_{ice} \sim 2.3$. Therefore, even one allows ion transmission ($f_i \neq 0$), the recycling of oxygen on the surfaces of grains, indicated by c_e, considerably extends the effective oxygen lifetime in the ring system.

Because the scale heights are a significant fraction of the width of the Cassini division, the variation in the ion column density though this region is smooth, unlike the simple model in Eq. (4b). Illumination through the Cassini gap also smoothes the variations in ion density over the B-ring on Saturn's sunward side and over the A-ring on the night side of Saturn. The decrease in ion density over the Cassini gap would appear to be consistent with the decrease in molecular oxygen column density in this region (Table 2). However, the lack of attenuation of the UV flux in the Cassini gap results in more efficient ionization north of the ring plane. If we use the nominal optical thickness and assume that ions are quenched when crossing the ring plane, $f_i = 0$, then the ion density on the shaded side of the ring *should be larger* over the Cassini gap than over the B-ring. Since the ion density in the shaded region depends on $(f_i + f)$, the relationship between these regions can be reversed if ion transmission occurs through the B-ring. Based on Eq. (4b) and assuming f_i^2 is small, the estimated column density at $R_p \sim 1.92R_S$ in the B-ring region using $m^* \neq 0$ in Fig. 4b implies that $c_e c_{ice}(f_i + f) \sim 10$. Since the optical thickness is ∼0.02, either the scattered light levels are significant, increasing the effective f, or significant ion transmission occurs in this region (i.e., $f_i \neq 0$).

A number of effects other than ion transmission might account for the observed relative ion densities near the Cassini gap. The extrapolation of the column density to the magnetic equator can be in error. However, at the spacecraft altitude the ion density is also seen to decrease in going through the Cassini gap. The size of the ratio of hydrogen to oxygen escape, c_e, can

vary across the ring plane, so that a global description of the transport and loss is needed, and there can be variations in the ring particle composition affecting the O_2 source rate. However, the trend in going from over the B-ring through the Cassini gap to over the inner edge of the A-ring strongly suggests to us that ion transmission is occurring.

We showed that the detection of significant ion densities by Cassini at altitudes that are many times the neutral scale height is due to ion-molecule scattering. Scattering also redistributes neutral molecules (Fig. 2). Therefore, scattering and dissociation can populate the magnetosphere with H, O, H_2, and O_2 outside of the main rings (Fig. 3). Although the photo-production rate, S_{O_2}, is small, the large surface area gives a net source $\sim 5 \times 10^{26}$ O/s as O or O_2 to the region outside of the rings. The precipitation of the energetic ions onto the edge of the A-ring would add to this. The ring source rate is comparable to the total water source rate needed by Jurac and Richardson (2005) to describe the OH torus inside the orbit of Mimas ($\sim 10^{27}$ O/s as H_2O, OH, O). The redistribution of O_2 by ion-molecule collisions is also consistent with the CAPS detection of O_2^+ outside the edge of the A-ring (Tokar et al., 2005), a radial extension of the O_2 ring atmosphere (Fig. 3). Since Cassini will not pass this close to the rings again during its nominal mission, but will explore regions affected by the escape of the O_2 ring atmosphere, simulations of the redistribution of atoms and molecules from the ring atmosphere are in progress (e.g., Johnson et al., 2005).

The surface-bounded atmosphere of Saturn's main rings, Europa, and other icy bodies in the Solar System arise from direct exposure of cold icy bodies to the space environment. Ultraviolet photons, plasma and energetic charged particles, and micrometeoroids are ubiquitous in such environments, so similar processes are involved and lead to production of atmospheres dominated by O_2 cycling many times between the surface ice and atmosphere. In the planetary magnetospheres the action of co-rotating planetary fields provides energy to ions, which then scatter neutral O_2 into the magnetospheric environment far beyond the source region possibly contributing to the oxygen plasma near Titan (Johnson et al., 2005). Oxygen produced from ice could also be a resource for astrobiology at Europa (Cooper et al., 2001; Chyba and Hand, 2001; Johnson et al., 2003) and elsewhere, but also may provide a false positive signature for photosynthesis. Thus the new findings for Saturn's toroidal ring atmosphere need to be compared to models for Europa's atmosphere for potential application to abiotic oxygen production on extrasolar planets to be investigated by future missions such as Terrestrial Planet Finder.

Acknowledgment

Work supported primarily by the Cassini Project under NASA/JPL contract 1243218 with SwRI. Work at the University of Virginia also supported by NASA's Planetary Atmosphere and Outer Planet Research Programs.

References

Bagenal, F., Sullivan, J.D., 1981. Direct plasma measurements in the Io torus and the inner magnetosphere of Jupiter. J. Geophys. Res. 86, 8447–8466.

Bouhram, M., Johnson, R.E., Berthelier, J.-J., Illiano, J.-M., Tokar, R.L., Young, D.T., Crary, F.J., 2005. A model of the atmosphere/ionosphere system of Saturn's main rings. Geophys. Res. Lett. Submitted for publication.

Brown, W.L., Augustyniak, W.M., Brody, E., Cooper, B., Lanzerotti, J.L., Ramirez, A., Evatt, R., Johnson, R.E., 1980. Energy dependence of the erosion of H_2O ice films by H and He ions. Nucl. Instrum. Methods 170, 321–325.

Brown, W.L., Augustyniak, W.M., Simmons, E., Marcantonio, K.J., Lanzerotti, L.J., Johnson, R.E., Boring, J.W., Reimann, C.T., Foti, G., Pirronello, V., 1982. Erosion and molecular formation in condensed gas films by electronic energy loss of fast ions. Nucl. Instrum. Methods B 1, 307–314.

Burger, M.H., Johnson, R.E., 2004. Europa's cloud: Morphology and comparison to Io. Icarus 171, 557–560.

Carlson, R.W., 1980. Photosputtering of Saturn's rings. Nature 283, 461–462.

Chenette, D.L., Cooper, J.F., Eraker, J.H., Pyle, K.R., Simpson, J.A., 1980. High-energy trapped radiation penetrating the rings of Saturn. J. Geophys. Res. 85 (A11), 5785–5792.

Chyba, C.F., Hand, K.P., 2001. Planetary science—Life without photosynthesis. Science 292, 2026–2027.

Cooper, J.F., 1983. Nuclear cascades in Saturn's rings: Cosmic ray albedo neutron decay and the origins of trapped protons in the inner magnetosphere. J. Geophys. Res. 88, 3945–3954.

Cooper, J.F., Eraker, J.H., Simpson, J.A., 1985. The secondary radiation under Saturn's A–B–C rings produced by cosmic ray interactions. J. Geophys. Res. 90, 3415–3427.

Cooper, J.F., Johnson, R.E., Mauk, B.H., Garrett, H.B., Gehrels, N., 2001. Energetic ion and electron irradiation of the icy Galilean satellites. Icarus 149, 133–159.

Esposito, L.W., and the UVIS Team, 2005. Ultraviolet imaging spectroscopy shows an active saturnian system. Science 307, 1251–1256.

Eviatar, A., McNutt Jr., R.L., Siscoe, G.L., Sullivan, J.D., 1983. Heavy ions in the outer Kronian magnetosphere. J. Geophys. Res. 88, 823–831.

Grun, E., Morfill, G.E., Terrile, R.J., Johnson, T.V., Schwehm, G., 1983. The evolution of spokes in Saturn's B-ring. Icarus 54, 227–252.

Hall, D.T., Strobel, D.F., Feldman, P.D., McGrath, M.A., Weaver, H.A., 1995. Detection of an oxygen atmosphere on Jupiter's moon Europa. Nature 373, 677–679.

Hansen, C.J., Shemansky, D.E., Hendrix, A.R., 2005. Cassini UVIS observations of Europa's oxygen atmosphere and torus. Icarus. In press.

Hill, T.W., Michel, F.C., 1976. Heavy ions from the Galilean satellites and the centrifugal distortion of the jovian magnetosphere. J. Geophys. Res. 81, 4561–4565.

Huebner, W.F., Keady, J.J., Lyon, S.P., 1992. Solar photo rates for planetary atmospheres and atmospheric pollutants. Appl. Space Sci. 195, 1–294.

Ip, W.-H., 1984. The ring atmosphere of Saturn: Monte Carlo simulations of the ring source model. J. Geophys. Res. 89, 8843–8849.

Ip, W.-H., 1995. Exospheric systems of Saturn's rings. Icarus 115, 295–303.

Ip, W.-H., 2000. Thermal plasma composition in Saturn's magnetosphere. Planet. Space Sci. 48, 775–783.

Ip, W.-H., 2005. An update on the ring exosphere and plasma disc of Saturn. Geophys. Res. Lett. 32, doi:10.1029/2004GL022217. L13204.

Johnson, R.E., 1990. Energetic Charged Particle Interaction with Atmospheres and Surfaces. Springer-Verlag, New York.

Johnson, R.E., 2002. Surface boundary layer atmospheres. In: Mendillo, M., Nagy, A., Waite, J.H. (Eds.), In: Atmospheres in the Solar System: Comparative Aeronomy Geophysical Monograph, vol. 130. Amer. Geophys. Union, Washington, DC, pp. 203–219.

Johnson, R.E., Quickenden, T.I., 1997. Photolysis and radiolysis of water ice on outer Solar System bodies. J. Geophys. Res. 102, 10985–10996.

Johnson, R.E., Lanzerotti, L.J., Brown, W.L., 1982. Planetary applications of condensed gas sputtering. Nucl. Instrum. Methods 198, 147–157.

Johnson, R.E., Quickenden, T.I., Cooper, P.D., McKinley, A.J., Freeman, C., 2003. The production of oxidants in Europa's surface. Astrobiology 3, 823–850. (Note: The G-value for Lyman-alpha induced production of O_2 is a factor of ten larger than in Table 2.)

Johnson, R.E., Carlson, R.W., Cooper, J.F., Paranicas, C., Moore, M.H., Wong, M.C., 2004. Radiation effects on the surface of the Galilean satellites. In: Bagenal, F., Dowling, T., McKinnon, W.B. (Eds.), Jupiter: The Planet,

Satellites and Magnetosphere. Cambridge Univ. Press, Cambridge, pp. 485–512. Ch. 20.

Johnson, R.E., Liu, M., Sittler, E.C., 2005. Plasma-induced clearing and redistribution of material embedded in planetary magnetospheres. Geophys. Res. Lett. In press.

Jurac, S., McGrath, M.A., Johnson, R.E., Richardson, J.D., Vasyliunas, V.M., Eviatar, A., 2002. Saturn: Search for a missing water source. Geophys. Res. Lett. 29. 2172, 25-1–4.

Jurac, S., Richardson, J.D., 2005. A self-consistent model of plasma and neutrals at Saturn: Neutral cloud morphology. Icarus. In press.

Krimigis, S.M., the MIMI Team, 2005. Dynamics of Saturn's magnetosphere from MIMI during Cassini's orbital insertion. Science 307, 1270–1274.

Luhmann, J.G., Johnson, R.E., Tokar, R.L., Cravens, T., 2005. A model of the ionosphere of Saturn's toroidal ring atmosphere. Icarus. Submitted for publication.

Luna, L., McGrath, M.A., Shah, M.B., Johnson, R.E., Liu, M., Latimer, C.J., Montenegro, E.C., 2005. Dissociative charge exchange and ionization of O_2 by fast H^+ and O^+ ions: Energetic ion interactions in the Europa's oxygen atmosphere and neutral torus. Astrophys. J. In press.

Maurice, S., Cooper, J.F., Johnson, R.E., Sittler, E.C., 2004. Sources for the radiation environment of Saturn's main rings and the Innermost Radiation Belt. AGU, Fall Meeting 2004. Abstract #P52A-03.

McGrath, M.A., Lellouch, E., Strobel, D.F., Feldman, P.D., Johnson, R.E., 2004. Satellite Atmospheres. In: Bagenal, F., Dowling, T., McKinnon, W.B. (Eds.), Jupiter: The Planet, Satellites & Magnetosphere. Cambridge Univ. Press, Cambridge, pp. 457–483. Ch. 19.

Noll, K.S., Rousch, T.L., Cruikshank, D.P., Johnson, R.E., Pendleton, Y.J., 1997. Detection of ozone on Saturn's satellites Rhea and Dione. Nature 388, 45–47.

Orlando, T.M., Sieger, M.T., 2003. The role of electron-stimulated production of O_2 from water ice in the radiation processing of outer Solar System surfaces. Surf. Sci. 528, 1–7.

Orlando, T.M., Grieves, G., 2005. Production of O_2 from ice by sub-band gap. In preparation.

Paranicas, C., Cheng, A.F., Mauk, B.H., Keath, E.P., Krimigis, S.M., 1997. Evidence for a source of energetic ions at Saturn. J. Geophys. Res. 102, 17459–17466.

Pospieszalska, M.K., Johnson, R.E., 1991. Micrometeorite erosion of the main rings as a source of plasma in the inner saturnian plasma torus. Icarus 93, 45–52.

Rye, R.R., Madey, T.E., Houston, J.E., Holloway, P.H., 1978. Chemical-state effects in Auger electron spectroscopy. J. Chem. Phys. 69, 1504–1512.

Sieger, M.T., Simpson, W.C., Orlando, T.M., 1998. Production of O_2 on icy satellites by electronic excitation of low-temperature water ice. Nature 394, 554–556.

Simpson, J.A., Bastian, T.S., Chenette, D.L., McKibben, R.B., Pyle, K.R., 1980. The trapped radiations of Saturn and their absorption by satellites and rings. J. Geophys. Res. 85, 5731–5762.

Shemansky, D.E., Hall, D.T., 1992. The distribution of atomic hydrogen in the magnetosphere of Saturn. J. Geophys. Res. 97, 4143–4161.

Shematovich, V.I., Johnson, R.E., Cooper, J.F., Wong, M.C., 2005. Surface-bounded atmosphere of Europa. Icarus 173, 480–498.

Smith, H.T., Johnson, R.E., Shematovich, V.I., 2004. Titan's atomic and molecular nitrogen tori. Geophys. Res. Lett. 31, doi:10.1029/2004GL020580.

Tokar, R.L., and 12 colleagues, 2005. Cassini Observations of the Thermal Plasma in the Vicinity of Saturn's Main Rings and the F and G Rings. Geophys. Res. Lett. 32, doi:10.1029/2005GL022690. L14S04.

Waite, J.H., Cravens, T.E., Ip, W.-H., Kasprzak, W.T., Luhmann, J.G., McNutt, R.L., Niemann, H.B., Yelle, R.V., Mueller-Wodarg, I., Ledvina, S.A., Scherer, S., 2005. Cassini ion and neutral mass spectrometer measurements of oxygen ions near Saturn's A-ring. Science. In press.

Westley, M.S., Baragiola, R.A., Johnson, R.E., Barrata, G.A., 1995. Ultraviolet photodesorption from water ice. Planet. Space Sci. 43, 1311–1315.

Young, D.T., and 43 colleagues, 2005. Composition and dynamics of plasma in Saturn's magnetosphere. Science 307, 1262–1268.

Yung, Y.L., McElroy, M.B., 1977. Stability of an oxygen atmosphere on Ganymede. Icarus 30, 97–103.